Design of Stimuli-Responsive Cobalt Tetraphenylporphyrinate-Chitosan Microspheres for Advanced Biosensors

European Journal of Inorganic Chemistry

EurJIC
European Journal of Inorganic Chemistry

Chemistry Europe
European Chemical Societies Publishing

RESEARCH ARTICLE OPEN ACCESS

Design of Stimuli-Responsive Cobalt Tetraphenylporphyrinate-Chitosan Microspheres for Advanced Biosensors

Domenica Marabello[1] | Paola Benzi[1] | Carlo Canepa[1] | Leonardo Mortati[2] | Giorgio Volpi[1] | Itzel M. Garnica-Palafox[3] | Francisco M. Sánchez-Arévalo[3] | Nadia A. Vázquez-Torres[3] | Alma Cioci[1]

[1]Dipartimento di Chimica, Università degli Studi di Torino, Torino, Italy | [2]Metrologia dei materiali innovativi e scienze della vita, Istituto Nazionale di Ricerca Metrologica, Torino, Italy | [3]Instituto de Investigaciones en Materiales, Universidad Nacional Autonoma de Mexico, Ciudad de México, México

Correspondence: Domenica Marabello (domenica.marabello@unito.it)

Received: 2 September 2025 | **Revised:** 11 November 2025 | **Accepted:** 13 November 2025

Keywords: biosensors | chitosan nanospheres | cobalt tetraphenylporphyrinate | nonlinear optics | photoresponsive crystals | theragnostics

ABSTRACT

In this work, we report the synthesis of new cobalt tetraphenylporphyrinate-chitosan-based microspheres for application as biosensors and in anticancer therapy. These microspheres were characterized using optical microscopy, scanning and transmission electron microscopy, and X-ray powder diffraction. We analyzed their nonlinear optical behavior, specifically the second harmonic generation (SHG), employing a high-resolution SHG microscope, with the quadratic fits of the SHG intensities considered as a function of the excitation power, under optimized experimental conditions. Beyond the typical porphyrinate fluorescence, the microspheres exhibit the same peculiar SHG behavior as CoTPP powder, making them suitable as multibiosensors. Additionally, they exhibit the same laser-induced dynamic properties previously observed in CoTPP powder, indicating their promising potential for dynamic anticancer therapies. The results of this work are encouraging, highlighting the possible application of these microspheres as multibiosensors and anticancer agents.

1 | Introduction

Porphyrins are macrocyclic heterocyclic organic compounds that are widely distributed in biological organisms. They exhibit prominent π-electron delocalization that is responsible for their peculiar chemical and physical properties. In particular, due to their remarkable fluorescence properties and biocompatibility, they have been widely studied and applied as biosensors [1–4]. They also exhibit a significant hyperpolarizability, which is responsible for the nonlinear optical (NLO) properties, particularly the second harmonic generation (SHG) and third (THG) harmonic generation (THG) properties, both currently under investigation for NLO bioimaging [5, 6].

SHG-based microscopy revolutionized the bio-imaging field by enabling noninvasive, high-resolution imaging in real time [7, 8], and SHG-based nanoprobes have been successfully employed for biological *in vitro* [9–12] and *in vivo* imaging [13, 14].

Reports concerning the NLO properties of porphyrinates in solution are scarce in the literature [6, 15, 16]. In our previous works, we investigated for the first time the SHG response of M(II)−5,10,15,20-tetraphenylporphyrinate (M═Co, Ni, Cu) in the solid state [17, 18]. We observed a remarkable enhancement of the SHG emission upon irradiating the powdered sample for a few minutes with a nanosecond Nd:YAG pulsed laser (1.907 μm). Specifically, the response of Co-5,10,15,20-tetraphenylporphyrinate (CoTPP) stimulated us to further explore this solid material for potential SHG biosensing applications. Furthermore, as a consequence of the irradiation, the magnetic moment of the powder of CoTPP increased by approximately three times, and the crystals blew up, scattering many crystalline fragments in the capillary.

In other words, the CoTPP crystals were photoresponsive; that is, they responded to an external laser light stimulus by an enhancement of the magnetic moment, and also by macroscopic mechanical motion (*dynamic crystals*) [19]. The enhancement of the magnetic moment is of particular interest for hyperthermia anticancer treatments. In these treatments, magnetic particles, encapsuled in cancer tissue, are heated by an alternating magnetic field [20]. Furthermore, to destroy cancer cells, magnetic nanoparticles can also be mechanically activated under a low-frequency magnetic field [20].

In this work, we propose the use of nanoparticles of CoTPP for diagnosis, due to their remarkable fluorescence and SHG properties, and for therapeutics, by exploiting their magnetic and SHG-dynamic properties; therefore, they can be proposed for multitheragnostic purposes. However, for biological applications, in order to drive the nanoparticles toward cells, it is necessary to cover them with a suitable biocompatible material that can be further functionalized to concentrate the nanoparticles in a specific tissue. In this work, we experimented with coating CoTPP nanoparticles with chitosan (CS), a very inexpensive, biocompatible, and nontoxic polysaccharide.

CS consists of β (1–4)-linked 2-amino-2-deoxy-D-glucose (D-glucosamine) and 2-acetamido-2-deoxy-D-glucosamine (N-acetyl-D-glucosamine) units, and it shows some structural similarities with glycosaminoglycans found in the extracellular matrix of several tissues [21, 22]. It is considered a versatile material for various biological applications, including the coating of solid nanoparticles that need to be introduced into biological cells [23, 24]. In fact, CS nanospheres have been proposed as drug delivery systems, due to their ability to be easily functionalized on their surface [25–27].

In our previous work [28], we developed the synthesis of CS-based nanospheres with Sr^{2+} ions encapsulated, for application as SHG biosensors, and concurrently as carriers of the ^{89}Sr radionuclide for radiopharmaceutical treatments in cancer therapy. The results encouraged us to attempt the encapsulation of porphyrinate-based particles within CS, allowing for the exploitation of the biosensing and therapeutic properties of the solid porphyrinates.

Thus, in this work, we report the synthesis of new CoTPP-chitosan-based microspheres (CoTPP-CS-MPs), characterized by X-ray powder diffraction (XRPD), optical microscopy, scanning electron microscopy (SEM), and transmission electron microscopy (TEM). Finally, their SHG behavior was investigated using a high-resolution SHG microscope, to explore their potential application as SHG biosensors and for anticancer therapeutic purposes.

2 | Results and Discussion

2.1 | Synthesis and Characterization of CoTPP-Loaded Chitosan-Based Microspheres (CoTPP-CS-MPs)

To obtain the CS-MPs, we used the oil in water (o/w) emulsion method previously reported in our work [28]. In addition, to prepare the o/w emulsion, we also tested a less dense oil, NF70, as a replacement for polyisobutylene. Due to its lower density, the cosmetic oil NF70 facilitated the diffusion of glutaraldehyde into the microspheres, thereby improving the reaction yield. Moreover, it is more cost-effective than polyisobutylene. As a result of this substitution, the total product mass increased significantly, shifting from a mode of 0.1 g to a mode of 2.5 g.

Figure 1 shows the optical microscopy images of the CS-MSs synthesized using polyisobutylene as oil and 0.9 w/v GA (Figure 1a), and those synthesized with NF70 and GA concentrations of 0.9, 0.4, and 0.2% w/v (Figure 1b–d, respectively). Considering the same amount of GA (Figure 1a,b), the microspheres produced with polyisobutylene are smaller and more homogeneous in size compared to the microspheres produced with NF70. However, the larger size of the microspheres synthesized with NF70 suggested the possibility of an easier loading of the CoTPP particles. Furthermore, the yield obtained using polyisobutylene was very low, whereas the yield using NF70 was 25-fold higher. For these reasons, we decided to proceed with the microspheres produced using NF70, optimizing the amount of GA added. Comparing Figure 1b–d, it is evident that a good compromise between yield and size homogeneity of the microspheres was achieved with the 0.4% w/v of GA (Figure 1c).

To prepare the CoTPP-CS-MPs, solid CoTPP was vigorously ground using a planetary ball mill. Figure 2 shows a SEM image of the resulting nanoparticles, where particle sizes ranging from 50 to 150 nm were measured. In Figure 3, the XRPD pattern of the CoTPP nanoparticles is compared to the XRPD pattern calculated from the single crystal X-ray structure (CCDC 2 130 187 [17]) to confirm that the sample was not degraded during the high-energy grinding. Even though the nanoparticles are in the nanometric range, the XRPD pattern does not show broadened peaks, indicating that no relevant defectivity is induced after grinding.

Before proceeding with the loading of CS-MPs with CoTPP, we evaluated the persistence of the nanoparticles in both the CS/PVA hydrogel and the mineral oils used for synthesis. Figure 4 shows optical microscope images of the CS/PVA hydrogel alone (Figure 4a) and the CoTPP nanoparticles suspended in the CS/PVA hydrogel (Figure 4b), in polyisobutylene (Figure 4c), and NF70 (Figure 4d). The images show that the CoTPP nanoparticles were not dissolved by the CS/PVA hydrogel or the mineral oils. Furthermore, the CoTPP nanoparticles suspended in NF70 (Figure 4d) are less agglomerated and more uniformly dispersed compared to those in polyisobutylene (Figure 4c).

To encapsulate the CoTPP into CS microspheres, a suspension of CoTPP nanoparticles in an aqueous solution of PVA was sonicated until it became homogeneous, and then the suspension was mixed with the CS solution to form the hydrogel. This hydrogel was used in place of the CS/PVA hydrogel previously used for the synthesis of the CS-MSs, following the same procedure. To confirm the encapsulation of the CoTPP nanoparticles within the CS matrix, TEM analysis was performed on both the unloaded CS-MPs and the CoTPP-loaded chitosan microspheres (CoTPP-CS-MPs) (Figure 5).

The TEM image of a CS microsphere in Figure 5a confirms the spherical morphology previously observed in our earlier work [28]. In contrast, Figure 5b shows that the presence of CoTPP nanoparticles affects the morphology of the CoTPP-CS-MP,

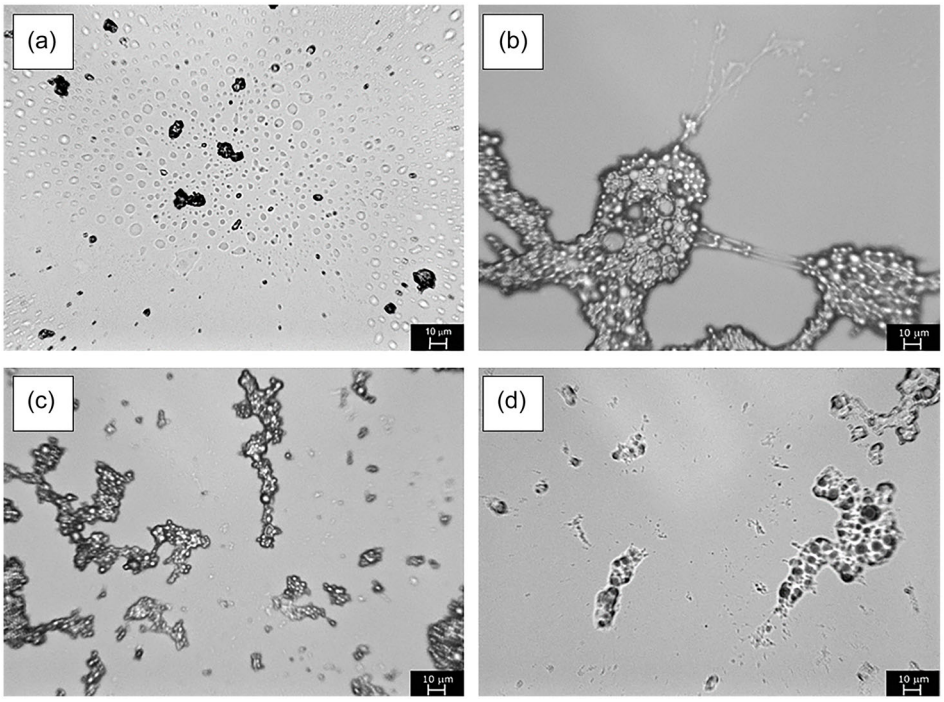

FIGURE 1 | (a) Optical microscopy images (40x magnification) of CS-MPs synthesized with polyisobutylene, (b) CS-MPs synthesized using NF70 and GA concentrations of 0.9% w/v, (c) 0.4% w/v, and (d) 0.2% w/V.

resulting in a less spherical shape. Nevertheless, the picture confirms that the metal-organic nanoparticles were successfully encapsulated within the CS matrix, as evidenced by the darker area at the center of the MP.

In order to optimize the yield of the microspheres' characteristics, different concentrations of CoTPP nanoparticles (1.0, 1.5, and 3.0% w/w) were tested. The highest concentration (3.0% w/w) led to a slight loss of CoTPP during the hexane washing step, as indicated by the pink coloration of hexane used to wash the CoTPP-CS-MPs. In the sample with 1.0% w/w of CoTPP, SEM-energy dispersive spectroscopy (EDS) analysis evidences a nonhomogeneous cobalt distribution (0.0%÷0.1%), close to the instrument detection limit. In contrast, the sample with 1.5% w/w of CoTPP showed a more uniform distribution, with values around 0.2%. Lastly, the sample with 3.0% w/w of CoTPP exhibited a nonuniform distribution: most areas had cobalt concentrations between 0.0%÷0.2% w/w, but larger aggregates were detected with cobalt levels around 5.1%, evidencing the sample heterogeneity. Based on these results, we concluded that the sample with the best features was the one synthesized with 1.5% w/w of CoTPP.

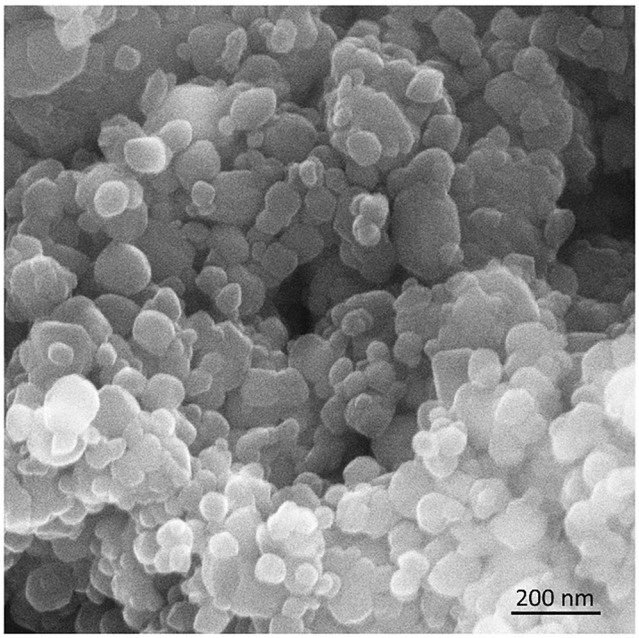

FIGURE 2 | SEM image of CoTPP nanoparticles after the milling process.

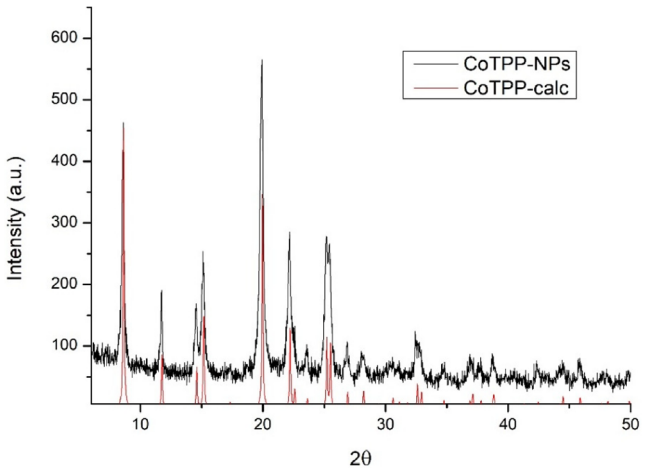

FIGURE 3 | XRPD pattern of CoTPP nanoparticles (black line), compared to the XRPD pattern calculated from the single crystal X-ray structure (red line).

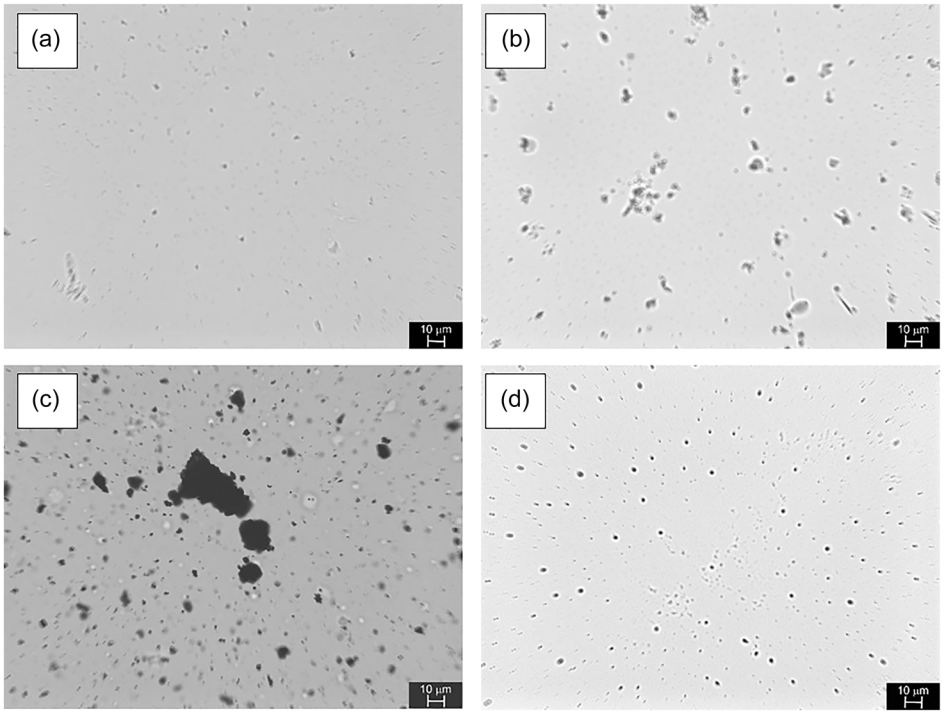

FIGURE 4 | (a) Optical microscopy images (40x magnification) of the CS/PVA hydrogel, (b) the CoTPP/CS/PVA suspension, (c) the CoTPP nanoparticles suspended in polyisobutylene, and (d) in NF70.

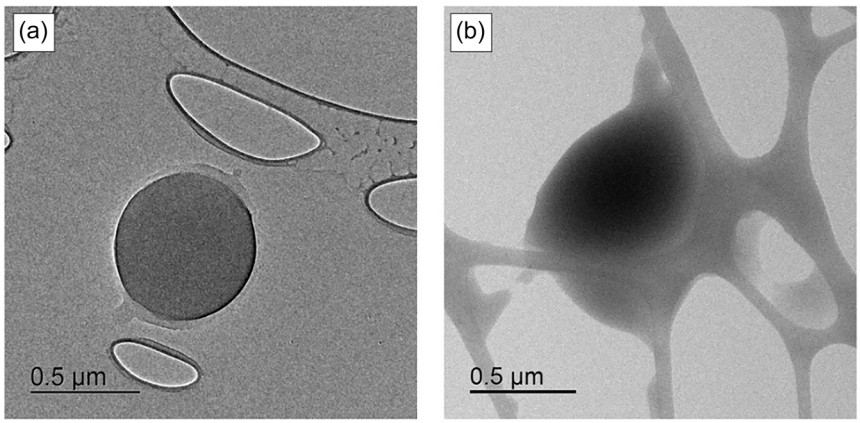

FIGURE 5 | (a) TEM images of CS-MPs and (b) CoTPP-CS-MPs with 1% w/w of CoTPP.

2.2 | Second Harmonic Generation Measurements

SHG measurements were performed on the CoTPP powder, the CS-MPs, and the CoTPP-CS-MPs synthesized with 1.5% w/w of CoTPP, as this sample exhibited the best characteristics in the TEM images. The efficiencies of the sample were compared to sucrose, as it is generally one of the standard compounds used for SHG measurements [29].

In our previous work [15], we described the peculiar behavior of the CoTPP powder under irradiation with a 1907 nm pulsed laser: during laser irradiation, a gradual increase of the intensity of the SH signal was observed until, after a few minutes, it reached a plateau of about 50 times the initial value. After this activation, the powder under irradiation was able to emit the SH light for a long time, directly starting from the plateau value. For this reason, CoTPP is a good candidate for the production of SHG bio-sensors. Furthermore, during irradiation, the powder's crystals jumped vigorously inside the capillary, demonstrating a prominent photodynamic property that could be exploited for eventual therapy against cancer cells.

In this work, we irradiated the samples with a 930 nm pulsed laser, since the SHG response is preferably in the visible spectrum (in this case, 465 nm) for bio-sensing applications. The CoTPP powder showed the same SHG behavior observed with the 1907 nm irradiation: initially, the intensity of the emitted SH had a lower magnitude than the sucrose, but after a few seconds with an excitation power of about 55 mW it considerably enhanced, starting from several points of the powder and spreading around each point, as if the impulses were propagated in the

area surrounding the starting point (see Supporting Information, Video 1). The SHG emission then remained stable, and the slight changes in the images were due to the movement of the powder's crystals. The movement of the crystals was so vigorous that it was necessary to cover the powder with a coverslip to avoid the loose of the sample. At the end of the experiment, an activated porphyrinate layer was deposited on the coverslip.

The CS-MPs, when irradiated, showed a mild SH emission, as expected [30], and the microspheres' shape was evident in the pictures (see Supporting Information, Video 2). However, after a few minutes, their SH emission suddenly disappeared, probably because the laser energy degraded them, and the image went completely dark. The CoTPP-CS-MPs, instead, showed behavior similar to the CoTPP powder (see Supporting Information, Video 3), except that the signal propagated throughout the sample more slowly, probably due to the lower concentration of CoTPP particles compared to the CoTPP powder, or also because the presence of the CS cover should limit the contact between the CoTPP particles. In any case, after a longer time, the SH intensity remains globally constant, except for the zones where the CoTPP particles moved away.

To achieve a more accurate estimation of the SHG efficiencies across various samples, the SHG signals produced by the samples were captured at 38 different excitation power levels. These SHG images were processed using a specialized algorithm, developed on the ImageJ platform, to extract the average intensity of the foreground objects for each power level. A quadratic fit was performed on these average values ($y = bx^2 + c$), yielding a parameter b that could be considered proportional to the characteristic effective hyperpolarizability β of the materials, and thus is related to the SHG efficiency of the material.

Measurements of the samples were performed at 930 nm, accounting for the effective excitation power at the sample. The photomultiplier (PMT) voltage was systematically adjusted from 500 to 1100 V in 100 V increments. This variation aimed to determine the most suitable experimental setup by minimizing the number of saturated pixels (which constrain the estimation of the true average SHG intensity) and maximizing the quality of the coefficient of determination (R^2) of the quadratic fit, used to derive the parameter b related to the material's hyperpolarizability. Figures S1–S4, Supporting Information, are reported the values of the extracted parameter b, of the coefficient of determination R^2 of the quadratic fit and the saturated pixel ratio, in function of the PMT voltage, and their explicit values when the PMT voltage was set to 800 V for each sample (Table S1, Supporting Information).

The average SHG intensity curves in Figure 6, displayed as a function of excitation power, clearly demonstrate the photo-activated CoTPP's strong SH property. This is especially evident when comparing the curve of the cobalt tetraphenylporphyrinate-chitosan-based microspheres (CoTPP-CS-MPs) to the relatively flat curve of the empty chitosan microspheres (CS-MPs), highlighting a significant enhancement.

Table 1 reports the ratios of the b values of the three samples (b_{sample}) with respect to the sucrose ($b_{sucrose}$) when the PMT voltage was 800 V (Figure S2, Supporting Information) and the fit goodness in terms of R^2 was above 0.94 (Figure S3, Supporting Information) and the prevalence of saturated pixel in the worst case was under 7.7% (Figure S4, Supporting Information). Analysis of the table reveals that the b parameter of CoTPP powder is twice as high as that of

TABLE 1 | The ratio of the SHG efficiency for the chitosan microspheres (CS-MPs), activated CoTPP into chitosan microspheres (CoTPP-CS-MPs), activated CoTPP powder (CoTPP powder) related to the parameter b of the sucrose using a PMT voltage of 800 V.

	Sucrose	CoTPP powder	CoTPP-CS-MPs	CS-MPs
$b_{sample}/b_{sucrose}$	1	2.065	0.431	0.013

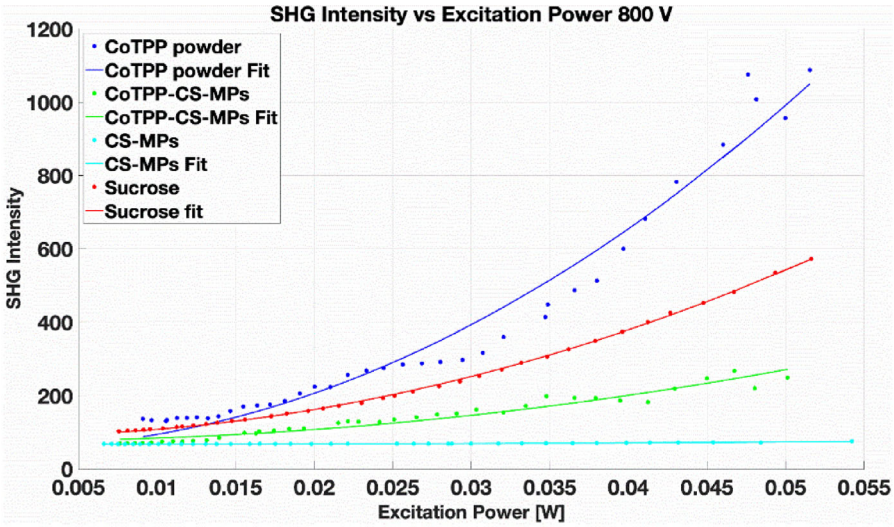

FIGURE 6 | SHG intensity versus excitation power 800 V of cobalt tetraphenylporphirinate-chitosan-based microspheres (CoTPP-CS-MPs synthesized with 1.5% w/w of CoTPP) compared to CoTPP powder, nondegraded empty chitosan microspheres (CS-MPs) and sucrose. Dotted lines represent the measurements, while the corresponding solid lines are the results of the fitting.

sucrose. The CoTPP-CS-MPs show an even more dramatic increase, with their *b* parameter being roughly 33 times greater than that of the empty CS-MPs, pointing to a substantial boost in SH properties.

3 | Summary and Conclusions

In this work, we successfully synthesized and characterized novel CoTPP-CS-based microspheres. Their formation was confirmed by optical and electron microscopies, as well as powder X-ray diffraction. Under optimal experimental conditions, we analyzed the SHG behavior of the activated CoTPP-CS-MPs, fitting the SHG intensities quadratically as a function of excitation power. This behavior was then compared with sucrose, activated CoTPP powder, and empty CS microspheres. The activated CoTPP-CS-MPs exhibited the same SHG behavior as the CoTPP powder, confirming their potential as SHG biosensors when suitably inserted into biological cells. Furthermore, we observed the same dynamic movement as the CoTPP powder, suggesting their applicability in dynamic cancer therapy. For future work, we plan to confirm that CoTPP-CS-MPs also possess the magnetic properties observed for the CoTPP powder. This will allow us to explore their potential application in magnetic anticancer therapies as well.

In conclusion, the results of this work are highly encouraging regarding the potential application of CoTPP-CS-based microspheres as multitheragnostic anticancer agents. Their fluorescence and high SHG emission properties can be exploited for multibiosensor applications, while their dynamic and potential magnetic properties offer avenues for multitherapeutic applications. Essentially, thanks to the nontoxicity of their components, these proposed microspheres could be explored for the new generation of anticancer therapies characterized by high damage to tumor cells and low side effects for the patient.

4 | Experimental

4.1 | Synthesis of Chitosan Microspheres (CS-MPs)

All chemicals utilized were purchased from Sigma–Aldrich and used as received. The acetic acid was HPLC-grade, and the CS powder was medium-molecular weight, with a 75%–85% degree of deacetylation. The poly(vinyl alcohol) (PVA) has a 99% degree of hydrolysis and a typical average molecular weight (Mw) of 89,000–98,000 g/mol.

CS powder was dissolved in a 1% w/v aqueous acetic acid solution, under magnetic stirring for 24 h at room temperature, resulting in a 2.5% w/v CS solution. PVA was dissolved in deionized water under magnetic stirring at 80°C for 2 h, to obtain a 10% w/v solution. The two polymeric solutions were then mixed at a CS:PVA volume ratio of 3:1, and magnetically stirred at room temperature for approximately 2 h, until a homogeneous polymeric blend was obtained.

A solution containing SPAN 80 (1% w/v) and either polyisobutylene or NF70 was stirred with an Ultra Turrax dispenser at 12,000 rpm. The CS/PVA polymeric blend was then slowly added drop by drop to form the microspheres. Finally, the crosslinker glutaraldehyde (GA, analytical grade, 50% w/v) water diluted at 0.9 w/v (b), 0.4 w/v, or 0.2 w/v, was added, and the emulsion was magnetically stirred for 40 min. After centrifugation of the emulsion, the polymeric hybrid CS/PVA/GA microspheres (CS-MPs) were collected at the bottom of the test tube and washed with two aliquots of hexane and two aliquots of deionized water. The CS-MPs were stored in water suspension to prevent particle agglomeration.

4.2 | Synthesis of CoTPP-Loaded Chitosan-Based Microspheres (CoTPP-CS-MPs)

CoTPP was purchased from PorphyChem. The powder of CoTPP was ground using a TMAX-DSP-LT01 planetary ball mill, equipped with 50 mL ZnO jars and ZnO balls with 4 mm diameter. The grinding parameters were set to 60 min at 500 rpm, using 8 min cycles alternating between clockwise and counterclockwise rotation, and with a 1 min break between cycles.

The resulting CoTPP particles were encapsulated in the CS matrix following the same procedure used to prepare the CS-MPs, except that the CoTPP particles were suspended in the CS/PVA polymeric blend. Different amounts of CoTPP (0.6, 1, 1.5, or 3% w/w) were added to the aqueous PVA solution and sonicated for 20–30 min. The resulting suspension was then mixed with the CS solution and added to the SPAN80-polyisobutylene emulsion to form the hydrogel microspheres (CoTPP-CS-MPs).

4.3 | Optical Microscopy

The optical microscope used to visualize the microspheres was an OMAX 40X-2500X Digital Lab Trinocular Compound LED Microscope, equipped with a 5MP Digital Camera.

4.4 | Scanning Electron Microscopy/Energy Dispersive Spectroscopy

Field-emission scanning electron microscopy (FESEM) and EDS were performed using a TESCAN S9000G FESEM 3010 microscope working at 30 kV and equipped with a high-brightness Schottky emitter. For microanalysis, the OXFORD Ultim Max-software Aztec was used. GIMP software [31] was used to obtain information on the dimensions of microparticles.

4.5 | Transmission Electron Microscopy

TEM microscopy was performed using a JEOL ARM-200F transmission electron microscope, Schottky emission type, operating at 80 pm in STME mode, and an acceleration voltage of 200 keV equipped with AGS166−3 Lacely carbon film 300 mesh Cu from Agar Scientific.

4.6 | X-Ray Powder Diffraction

The diffraction pattern was collected using a Bruker D8 Advance diffractometer equipped with Ni-filtered Cu-Kα radiation

($\lambda = 1.5406$ Å). All patterns were recorded over a 2θ range of 5°÷70°, with a scan rate of 0.4 °/min.

4.7 | Second Harmonic Generation Measurements

The SHG efficiency of the samples was assessed in comparison to sucrose powder, using an upright microscope (BX51WI, Olympus, Tokyo, Japan) paired with a scanning unit (FluoView FV300, Olympus, Tokyo, Japan). The SHG signal was detected by scanning the samples point by point with high resolution and excitation efficiency through an objective lens (UPLSAPO 20x, NA = 0.75, Olympus). The excitation source was a pulsed output tuned to 930 nm, with a pulse duration of ≈2 ps and a repetition rate of 80 MHz, generated by an Optical Parametric Oscillator (Levante Emerald OPO) (APE, Berlin, Germany). The oscillator was pumped by a Yb-fiber laser (Emerald Engine HP, APE, Berlin, Germany) emitting at ≈516 nm, also with a pulse duration of around 2 ps and a repetition rate of 80 MHz.

The SHG signal, detected around 465 nm, was optically filtered within the range of 330–480 nm (using FF01-405/150 Semrock) and collected in a back-scattering (epi-detection) configuration via one of two PMT detectors located in the microscope scanning head. The same PMT gains, voltages, and offset settings were applied for all samples.

The CoTPP powder was simply spread on the slide, while for the CS-MPs and the CoTPP-CS-MPs, a drop of the suspension was placed on a glass microscope slide and allowed to dry. Before the samples were examined under the microscope, a rectangular coverslip was adhered to each slide to avoid the eventual dispersion of the samples.

Acknowledgments

This study was financed by the European Union - Next Generation EU, Missione 4 Componente 1 CUP D53D23010380006. F. M. Sánchez-Arévalo is grateful for the partial financial to this research, from PAPIIT DGAPA-UNAM program through the grant IN101624. Nadia A. Vázquez Torres acknowledgments DGAPA postdoctoral fellowship grant.

Open access publishing facilitated by Universita degli Studi di Torino, as part of the Wiley - CRUI-CARE agreement.

Funding

This study was supported by European Union (Next Generation EU, Missione 4 Componente 1 CUP D53D23010380006), Universidad Nacional Autonoma de México (PAPIIT DGAPA-UNAM program, grant IN101624), and Universidad Nacional Autonoma de México (DGAPA postdoctoral fellowship grant).

Conflicts of Interest

The authors declare no conflicts of interest.

Data Availability Statement

The data that support the findings of this study are available from the corresponding author upon reasonable request.

References

1. G. Pandey, R. Chaudhari, B. Joshi, S. Choudhary, J. Kaur, and A. Joshi, "Fluorescent Biocompatible Platinum-Porphyrin–doped Polymeric Hybrid Particles for Oxygen and Glucose Biosensing," *Scientific Reports* 9 (2019): 5029–5040.

2. K. Norvaiša, M. Kielmann, and M. O. Senge, "Porphyrins as Colorimetric and Photometric Biosensors in Modern Bioanalytical Systems," *ChemBioChem* 21 (2020): 1793–1807.

3. M. Imran, M. Ramzan, A. K. Qureshi, M. A. Khan, and M. Tariq, "Emerging Applications of Porphyrins and Metalloporphyrins in Biomedicine and Diagnostic Magnetic Resonance Imaging," *Biosensors* 8 (2018): 95–111.

4. S. Chandra, C. Mende, D. Bahadur, A. Hildebrandt, and H. Lang, "Fabrication of a Porphyrin-Based Electrochemical Biosensor for Detection of Nitric Oxide Released by Cancer Cells," *Journal of Solid State Electrochemistry* 19 (2015): 169–177.

5. A. Khadria, J. Fleischhauer, I. Boczarow, J. D. Wilkinson, M. M. Kohl, and H. L. Anderson, "Porphyrin Dyes for Nonlinear Optical Imaging of Live Cells," *IScience* 4 (2018): 153–163.

6. J. E. Reeve, H. A. Collins, K. D. Mey, et al., "Amphiphilic Porphyrins for Second Harmonic Generation Imaging," *Journal of the American Chemical Society* 131, no. 8 (2009): 2758–2759.

7. M. J. Therien, "How to Improve Your Image," *Nature* 458 (2009): 716–717.

8. L. Sacconi, D. A. Dombeck, and W. W. Webb, "Overcoming Photodamage in Second-Harmonic Generation Microscopy: Real-Time Optical Recording of Neuronal Action Potentials," *Proceedings of the National Academy of Sciences of USA* 103 (2006): 3124–3129.

9. A. Kachynski, A. Kuzmin, M. Nyk, I. Roy, and P. N. Prasad, "Zinc Oxide Nanocrystals for Non-Resonant Nonlinear Optical Microscopy in Biology and Medicine," *Journal of Physical Chemistry C* 112 (2008): 10721–10724.

10. T. R. Kuo, C. L. Wu, C. T. Hsu, et al., "Chemical Enhancer Induced Changes in the Mechanisms of Transdermal Delivery of Zinc Oxide Nanoparticles," *Biomaterials* 30 (2009): 3002–3008.

11. C. L. Hsieh, R. Grange, Y. Pu, and D. Psaltis, "Three-Dimensional Harmonic Holographic Microcopy Using Nanoparticles as Probes for Cell Imaging," *Optics Express* 17 (2009): 2880–2891.

12. J. Extermann, L. Bonacina, E. Cuña, et al., "Nanodoublers as Deep Imaging Markers for Multi-Photon Microscopy," *Optics Express* 17 (2009): 15342–15349.

13. P. Pantazis, J. Maloney, D. Wu, and S. E. Fraser, "Second Harmonic Generating (SHG) Nanoprobes for In Vivo Imaging," *Proceedings of the National Academy of Sciences of USA* 107 (2010): 14535–14540.

14. G. Malkinson, P. Mahou, É. Chaudan, et al., "Fast In Vivo Imaging of SHG Nanoprobes with Multiphoton Light-Sheet Microscopy," *ACS Photonics* 7 (2020): 1036–1049.

15. F. Tessore, G. Di Carlo, A. Forni, S. Righetto, F. Limosani, and A. Orbelli Biroli, "Second Order Nonlinear Optical Properties of 4-Styrylpyridines Axially Coordinated to A_4 Zn^{II} Porphyrins: A Comparative Experimental and Theoretical Investigation," *Inorganics* 8, no. 8 (2020): 45–57.

16. G. Di Carlo, M. Pizzotti, S. Righetto, A. Forni, and F. Tessore, "Electric-Field-Induced Second Harmonic Generation Nonlinear Optic Response of A_4 β-Pyrrolic-Substituted Zn^{II} Porphyrins: When Cubic Contributions Cannot Be Neglected," *Inorganic Chemistry* 59 (2020): 7561–7570.

17. P. Antoniotti, C. Canepa, E. Cariati, et al., "The Peculiar SHG Behaviour of Co-5,10,15,20-Tetraphenilporphyrinate in the Solid State. An Experimental and Theoretical Study," *Journal of Molecular Structure* 1294 (2023): 136340–136349.

18. A. Cioci, P. Antoniotti, P. Benzi, et al., "SHG Behavior of the Solid Isomorphic Compounds Ni- and Cu-5,10,15,20- Tetraphenylporphyrinate. An Experimental and Theoretical Study," *Journal of Molecular Structure* 1317 (2024): 139201–139212.

19. P. Naumov, D. P. Karothu, E. Ahmed, et al., "The Rise of the Dynamic Crystals," *Journal of the American Chemical Society* 142 (2020): 13256–13272.

20. H. S. Huang and J. F. Hainfeld, "Intravenous Magnetic Nanoparticle Cancer Hyperthermia," *International Journal of Nanomedicine* 8 (2013): 2521–2532.

21. J. A. Benítez-Martínez, MGarnica-Palafox l., G. Vázquez-Victorio, M. Hautefeuille, and F. M. Sánchez-Arévalo, "Semi-Interpenetrating Polymeric Networks Based on Poly(dimethylsiloxane)-Chitosan-Poly (vinyl Alcohol) Crosslinked with Genipin with Possible use in Biomedical Applications," *Journal of Materials Science* 56 (2009): 1–20.

22. I. M. Garnica-Palafox and F. M. Sánchez-Arévalo, "Influence of Natural and Synthetic Crosslinking Reagents on the Structural and Mechanical Properties of Chitosan-Based Hybrid Hydrogels," *Carbohydrate Polymers* 151 (2016): 1073–1081.

23. L. A. Frank, G. R. Onzi, A. S. Morawski, A. R. Pohlmann, S. S. Guterres, and R. V. Contri, "Chitosan as a Coating Material for Nanoparticles Intended for Biomedical Applications," *Reactive Functional Polymers* 147 (2020): 104459–104472.

24. J. Ji, S. Hao, D. Wu, R. Huang, and Y. Xu, "Preparation, Characterization and In Vitro Release of Chitosan Nanoparticles Loaded with Gentamicin and Salicylic Acid," *Carbohydrate Polymers* 85 (2011): 803–808.

25. R. Pandey and G. Mathur, "Current Trends in Chitosan Functionalization Methods and Their Applications," *Starch* 77 (2025): 2300248–2300255.

26. R. Wu, A. S. Abdulhameed, S. K. Yong, et al., "Functionalization of chitosan biopolymer with SiO_2 nanoparticles and benzaldehyde via hydrothermal process for acid red 88 dye adsorption: Box-Behnken design optimization.," *International Journal of Biological Macromolecules* 247 (2023): 125806–125818.

27. F. Tang, L. Zhang, J. Zhu, Z. Cheng, and X. Zhu, "Surface Functionalization of Chitosan Nanospheres via Surface-Initiated AGET ATRP Mediated by Iron Catalyst in the Presence of Limited Amounts of Air," *Industrial and Engineering Chemistry Research* 48 (2009): 6216–6223.

28. A. Cioci, P. Benzi, C. Canepa, et al., "Fructose-Based Metal–Organic Framework as a Means to Synthesize Sr-Loaded Chitosan Nanospheres with NLO Properties for Theranostic Applications in Radiotherapy," *Inorganics* 12 (2024): 231–250.

29. S. K. Kurtz and T. T. Perry, "A Powder Technique for the Evaluation of Nonlinear Optical Materials," *Journal of Applied Physics* 39 (1968): 3798–3813.

30. E. Praveen, S. Murugan, and K. Jayakumar, "Investigations on the Existence of Piezoelectric Property of a Bio-Polymer-Chitosan and Its Application in Vibration Sensors," *RSC Advances* 7 (2017): 35490–35495.

31. GNU Image Manipulation Programme, GIMP V 2.6.6. https://www.gimp.org/.

Supporting Information

Additional supporting information can be found online in the Supporting Information section. **Supporting Fig**. **S1:** Quadratic coefficient *vs* PMT (Photo-Multiplier Tube) voltage of Cobalt tetraphenylporphirinate-chitosan based microspheres (CoTPP-CS-MPs) compared to CoTPP powder, empty chitosan microspheres (CS-MPs) and sucrose. **Supporting Fig. S2:** Normalized quadratic coefficient *vs* PMT voltage of Cobalt tetraphenylporphirinate-chitosan based microspheres (CoTPP-CS-MPs) compared to CoTPP powder, empty chitosan microspheres (CS-MPs) and sucrose. **Supporting Fig. S3:** Quadratic fit coefficient of determination R2 *vs* PMT voltage of Cobalt tetraphenylporphirinate-chitosan based microspheres (CoTPP-CS-MPs), compared to CoTPP powder, empty chitosan microspheres (CS-MPs) and sucrose. **Supporting Fig. S4:** Saturated pixels ratio *vs* PMT voltage of Cobalt tetraphenylporphirinate-chitosan based microspheres (CoTPP-CS-MPs) compared to CoTPP powder, empty chitosan microspheres (CS-MPs) and sucrose. **Supporting Table S1:** Parameters obtained from the image acquisitions, using PMT voltage at 800 Volts, of the quadratic fit *b* ratios related to the sucrose, the fits' coefficients of determination R2, and the saturated pixel ratio percentages for cobalt tetraphenylporphirinate-chitosan based microspheres (CoTPP-CS-MPs), CoTPP powder, empty chitosan microspheres (CS-MPs) and sucrose. **Supporting Video S1**. **Supporting Video S2**. **Supporting Video S3**.